Energy 333 (2025) 137473

Contents lists available at ScienceDirect

Energy

journal homepage: www.elsevier.com/locate/energy

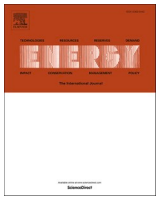

Design optimization of road thermal collectors: A numerical and experimental study in the Mediterranean

Alessandro Buscemi *, Stefania Guarino, Alessandro Biondi, Marco Beccali, Valerio Lo Brano

Department of Engineering, University of Palermo, Viale delle Scienze, Palermo, Italy

ARTICLE INFO

Keywords:
Road thermal collectors
Thermal response tests
Finite element modelling
Plant performance assessment
Parametric analyses

ABSTRACT

Roads, car parks, and airport runways constitute some of the largest, but least utilized, solar thermal surfaces in urban areas. Roads thermal collectors can exploit this resource to reduce the effects of urban heat islands and decarbonize low-temperature heat demand by powering building-level heat pump systems. This study presents a two-dimensional numerical model using the finite element method to simulate collector performance. It introduces a novel approach to calculate convective heat transfer coefficients based on wind speed and atmospheric stability, validated against experimental data from an 80 m^2 prototype at the University of Palermo, Italy. The prototype features heat exchanger tubes 14.5 cm below the asphalt within a thermally conductive concrete layer, mirroring urban road construction to reduce costs and maintenance. A 50-cm lightweight insulating concrete layer was also included to boost efficiency. The model enabled parametric analyses of 18 collector configurations, varying tube spacing, insulation thickness, and concrete conductivity. Results show that while an insulating layer increases peak thermal output, it does not significantly improve seasonal energy collection. Reducing tube spacing, however, enhances both peak output and total energy harvested. An optimized design with 20 cm tube spacing and no insulating layer is projected to achieve 320 kWh/m^2 annually in Palermo, with a 25 % seasonal solar-to-thermal conversion efficiency, assuming a 20 °C inlet water temperature.

1. Introduction

Globally, approximately 17.5 % of greenhouse gas emissions can be attributed to the energy demands of buildings [1]. A review of the data from 2022 indicates that over 50 % of the energy consumed in buildings is used for heating and hot water production and two-thirds of this energy is still generated using fossil fuels [2]. In order to achieve a net-zero emission building sector, it will be necessary to reduce the energy demand of existing and new buildings, as well as to implement policies to promote the electrification and direct use of renewable energy for heating and cooling [3]. To this end, one of the most promising strategies for heating buildings is to use heat pumps combined with sensible heat storage systems powered by solar thermal energy [4]. In cold climate zones, among the most efficient combinations for heating buildings in addition to ground source heat pump systems [5] are those integrating borehole thermal energy storages with water-to-water heat pumps and evacuated tube solar collectors [6].

In some specific cases, it may be interesting to study the possibility of implementing an alternative configuration of this type of layout, in which road thermal collectors replace traditional solar collectors. A study of this type is currently underway for a pilot plant integrating an RTC and a borehole thermal energy storage with the aim of emulating the operation of the heating system of a hypothetical non-residential building in the Mediterranean area [7]. Road thermal collector systems are realized by embedding heat exchanger pipes in the asphalt layers of roads and car parks [8], taking advantage of the high capacity of asphalt to absorb solar radiation and the possibility to easily realize large solar energy collection surfaces [9]. RTCs belong to the wider family of hydronic asphalt pavement systems [10], which have a variety of applications, including preventing snow and ice accumulation on road surfaces in continental regions [11] and mitigating the urban heat island effect [12] in warmer locations [13]. It is important to note that HAPs are distinguished both by their use and the lesser depth of their

This article is part of a special issue entitled: SDEWES 2024 published in Energy.

* Corresponding author.
E-mail addresses: alessandro.buscemi@unipa.it (A. Buscemi), stefania.guarino@unipa.it (S. Guarino), alessandro.biondi@unipa.it (A. Biondi), marco.beccali@unipa.it (M. Beccali), valerio.lobrano@unipa.it (V. Lo Brano).

https://doi.org/10.1016/j.energy.2025.137473
Received 20 December 2024; Received in revised form 6 June 2025; Accepted 7 July 2025
Available online 8 July 2025

Nomenclature

Symbols

a	solar absorptance, [−]
A	surface area, [m^2]
c	specific heat, [$J{\cdot}kg^{-1}{\cdot}K^{-1}$]
D	diameter, [m]
G	global horizontal irradiance, [$W{\cdot}m^{-2}$]
h	convective heat transfer coefficient, [$W{\cdot}m^{-2}{\cdot}K^{-1}$]
L	length, [m]
$\dot{m}$	mass flow rate, [$kg{\cdot}s^{-1}$]
N	total number of sample in a dataset
v	speed, [$m{\cdot}s^{-1}$]
$\dot{q}$	heat flux per unit of surface, [$W{\cdot}m^{-2}$]
R	convective thermal resistance (per unit of length), [$m{\cdot}K{\cdot}W^{-1}$]
RH	relative humidity, [%]
ro	average surface roughness, [−]
T	temperature, [K]
y	actual or predicted value of a target variable
z	height, [m]

Subscript

a	asphalt-binder
air	air
$cond$	conductive
$conv$	convective
f	fluid
h	horizontal
i	inner
j	number of a sample in a dataset
p	pipe
rad	radiative
ref	reference
ru	rural
s	solid
sky	sky
sun	solar
ur	urban
wi	wind

Greek letters

α	thermal diffusivity, [$m^2\ s^{-1}$]
β	the power-law exponent of Equation (11), [−]
ε	long-wave emissivity, [−]
λ	thermal conductivity, [W/(m·K)]
ρ	bulk density, [kg/m^3]
σ	Stefan–Boltzmann constant, 5.67 × 10−8 [$W\ m^{-2}\ K^{-4}$]

Acronyms

BTES	Borehole Thermal Energy Storage
FE	Finite Element
FEM	Finite Element Method
GSHP	Ground Source Heat Pump
HAP	Hydronic Asphalt Pavement
HTF	Heat Transfer Fluid
MAE	Mean Absolute Error
MAPE	Mean Absolute Percentage Error
ODE	Ordinary Differential Equation
PDE	Partial Differential Equation
RTC	Road Thermal Collector
SMARTEP	Sustainable Model and Renewable Thinking Energy Parking
TMY	Typical Meteorological Year
TRT	Thermal Response Test

pipes from horizontal ground heat exchangers [14] used in GSHP systems [15]. While road thermal collectors are simply hydronic asphalt pavement that operate mainly in the summer season to produce thermal energy from solar sources [16].

From the perspective of the principal design parameters, several studies have demonstrated that the laying depth and the spacing between heat exchanger pipes have a significant impact on the efficiency of RTCs and the thermal levels of heat produced by them [16]. In particular, the placement of the pipes at a greater depth results in a more uniform temperature distribution, although this does have an adverse effect on the efficiency of the collector [17]. Conversely, the placement of the tubes in closer proximity reduces the temperature of the heat transfer fluid, which is mainly related to the formation of a "cold" spot between the tubes [18]. However, this does have the beneficial effect of increasing the efficiency of road thermal collectors.

From a construction point of view, arranging the pipes too close together can lead to poor compaction of the asphalt between them. Additionally, placing pipes shallowly from the surface increases the potential for damage from passing vehicles [10]. A recent review of over 50 large-scale designs of HAPs reveals that the majority of these systems arrange the pipes at a depth of between 5 and 7 cm, with an inter-distance between tube centers ranging from 10 to 25 cm [10]. The same study indicates that the energy-harvesting capacity of these collectors ranges from 0.6 to 0.8 GJ/m^2/year, with solar-to-thermal conversion efficiencies ranging from 20 % to 50 %, depending on the construction characteristics and geographic location.

Several numerical approaches have been developed to study dynamic operation of road thermal collectors: 2D models of a road heat rejecter [19] and a snow-melting system [20], 3D hybrid models [21], full 3D models [22] of HAPs. In all these models, a crucial aspect is the definition of the surface energy balance that is imposed as an upper boundary condition [23]. Among the most recently constructed RTC pilot plants, for which new numerical models have also been developed, are.

- the 150 m^2 collector constructed on an access road in Toddington, UK [24]. The collector consists of an array of cross-linked polyethylene tubes, 2.5 cm in diameter and 30 m long, which are placed at a depth of 12 cm from the road surface, with a spacing of 25 cm between each tube. The pilot site was monitored for about two years and a computational fluid dynamics model was developed using the commercial software PHOENIX to simulate the operation of the collector.
- the 70 m^2 collector in Östersund, Sweden realized with a concrete pavement where the pipes, spaced 5 cm apart, are placed 6.2 cm deep. A 10 cm layer of thermal insulation material is placed below to provide a more stable boundary condition for comparison with the numerical simulation results [21]. A new numerical model (HyRoSim) was developed for this system.
- The 65 m^2 system installed in Antwerp [25], Belgium, in which the pipes are placed 4.5 cm above the surface with a distance between them of 15 cm [26]. A 3D finite element model (implemented using COMSOL Multiphysics® [27]) and a simplified model (based on energy flows and heat balance) were developed for this case.

Finally, among the few other examples of pilot plants built to harvest heat from the asphalt of a road, is the GAIA system [28].

- this snow-melting system in Ninohe, Japan, is a 266 m^2 collector constructed using 64 m long, 16 mm-internal-diameter polybutene pipes embedded in asphalt concrete pavement at 20 cm intervals. The pipes are positioned to a depth of 10 cm from the surface of the pavement. Monitoring of the system when fully operational showed an average heat recovery rate per unit collector area of between 92 and 113 W/m^2.

The above summary of the existing literature analysis shows that there are some gaps in the research on this interesting type of solar collector, including the following.

- The majority of large-scale road thermal collectors were constructed in continental regions, with very few located in the Mediterranean area [10].
- Although a recent experimental-numerical study [29] shows that wind speed has a significant impact on the efficiency and thermal response of road thermal collectors, relatively few studies have modelled this effect.
- No thermal response tests have been defined for this type of solar collector, similar to what has already been developed for horizontal ground heat exchangers [30].

This work refers to a new road thermal collector occupying 80 m^2 of a car park on the campus of the University of Palermo, Italy [7]. This system, implemented as part of the SMARTEP project [31], has the following features.

- the heat exchanger pipes are inserted at a depth of 14 cm, in a thermally conductive concrete layer below the asphalt-binder layer, and are spaced 14.5 cm apart.
- a layer of thermally insulating material, made of lightweight concrete, was placed on top of the conductive layer to reduce thermal losses to the base soil.

This system differs from other road thermal collectors due to the deeper installation of the pipes and the presence of the lower insulation, which, unlike the Östersund system [21], was designed to increase the collector's peak heat output power. The purpose of this design was to create a low-cost system for installation and maintenance with a construction stratigraphy as close as possible to a conventional road pavement [31]. Two cross-sections of the RTC were equipped with thermal sensors to monitor the temperatures of its different layers in real time, every 10 min. The data collected during the initial 43 days following construction (without water circulation in the pipes) were analyzed using a novel methodology based on a one-dimensional finite element model [7]. This approach was employed to characterize the thermophysical properties of all materials.

This paper reports on the progress of experimental and numerical activities aimed at energy analyses of the new RTC of Palermo. In particular, it presents.

- a new two-dimensional FE model of a road heat collector has been developed, building upon the models originally proposed in Ref. [19] and later extended in Ref. [20]. This enhanced model introduces advancements in the representation of radiative and convective heat exchanges at the asphalt–atmosphere interface [32], incorporating recent literature-based correlations for sky temperature estimation and a novel approach that accounts for atmospheric stability effects in defining wind speed,
- experimental results of two thermal response tests executed on the RTC (with circulation of water in the pips) which were used to preliminarily validate the numerical model.

The validated numerical model was then used to perform parametric simulations aimed at validating the current design of the Palermo collector and identifying its possible optimized configuration. These simulations were carried out by varying the distance between the pipes, the thickness and the thermophysical properties of the lightened concrete insulation layer. It is worth noting that, to define these properties, new correlations were used in the model that relate the thermal conductivity of this type of material to its bulk density.

2. Materials and methods

This section describes the FE model developed for the RTC, the main characteristics of the RTC of Palermo, and the TRTs carried out on the collector. It also outlines the configurations defined for the parametric analyses to identify an optimized system.

2.1. The new finite element model defined for road thermal collectors

Inspired by models developed by Ref. [19] to simulate the operation of HAPs used to prevent snow and ice accumulation on road surfaces, a two-dimensional FE model of the road thermal collector (implemented with COMSOL Multiphysics®) was developed. Fig. 1 describes the conceptual procedure by which the representative reduced two-dimensional domain of the RTC was defined. The assumptions of the proposed simplified approach are as follows.

- the heat flux exchanged per linear meter between the conductive layers of the RTC and the pipes embedded in them can be assumed to be approximately constant along the entire extension of the pipes (which implies that the temperature distribution of HTF along the tubes is approximately linear).

- In each cross-section of the collector (i.e. orthogonal to the longest direction), the temperature field of the RTC around one heat exchanger tube can be assumed to be similar to that of all the others, since the different pipes are hydraulically supplied in parallel.

- The effect of the side-boundaries of the road thermal collector on the average temperature distribution around each tube can be considered negligible.

In other words, the representative two-dimensional model makes it possible to calculate the average temperature distribution in the central cross-section of the solar collector.

For this purpose, the boundary conditions imposed on the calculation domain are as follows.

- on the upper boundary the net heat flux resulting from the energy balance [7] at the atmosphere-asphalt interface was imposed as boundary condition (see Fig. 2). This heat flux depends non-linearly on the surface temperature of the asphalt T_a, which is itself an unknown in the problem.
- On the lower boundary, temperature values (Dirichlet condition) were imposed equal to those that would occur over time in the undisturbed soil at that depth.

- Along the two side boundaries, which can be considered as axes of symmetry, a zero heat flow was imposed.

- Along the section of the domain curve coinciding with the inner wall of the pipe, a mixed temperature and heat flux condition is imposed, where the temperature of the inner wall $T_{p,i}$ (unknown) is assumed to be uniform on the same boundary and the heat flux is equal to that exchanged with the fluid circulating in the pipes.

To model the first and last of the complex boundary conditions listed above, the general extrusion operators and the custom boundary weak form available in COMSOL Multiphysics® [27] were used. The FE model

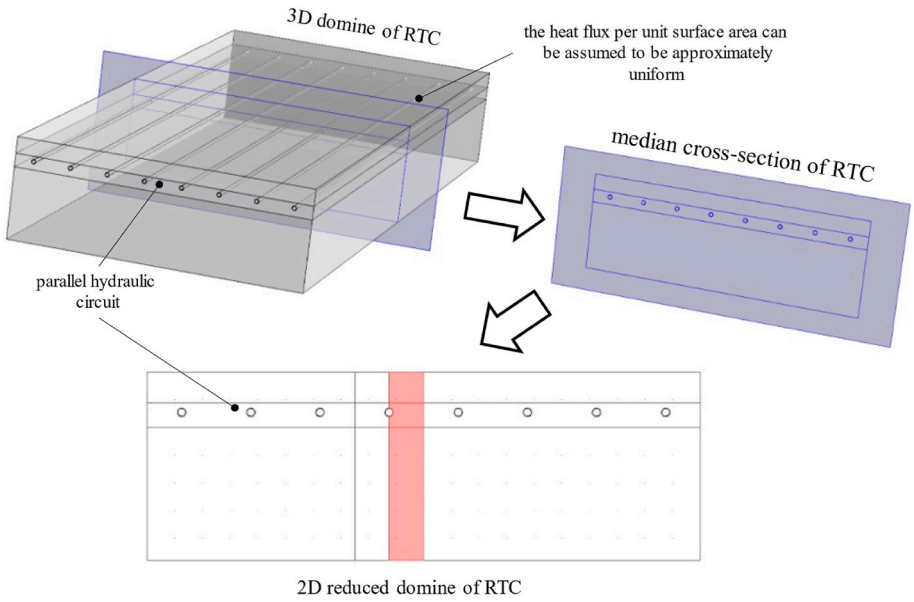

Fig. 1. Conceptual procedure, leading to the definition of a reduced 2D representative domain of an RTC system.

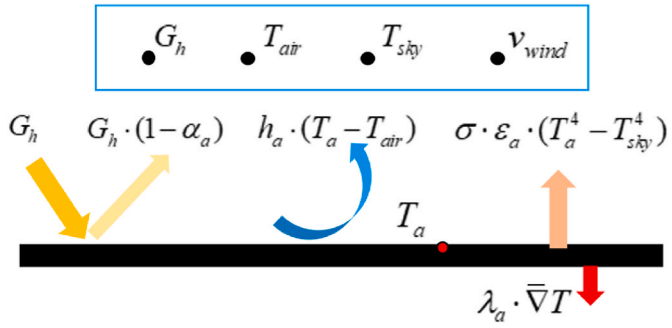

Fig. 2. Surface energy balance at the RTC-atmosphere interface.

allows the scalar field of temperature $T(x,y)$ to be calculated for each of the solid domains constituting road thermal collector by numerically solving the following partial differential equation, which represents the conservation of enthalpy in each of the same domains, under the assumption of heat flow by conduction:

$$\rho \cdot c \cdot \frac{dT}{dt} = \nabla \cdot (\lambda \cdot \overline{\nabla} T) \tag{1}$$

where ρ is the density, c the specific heat and, λ the thermal conductivity of the solid material. These thermophysical parameters must be defined for each material constituting the RTC.

Moreover, the following ordinary differential equation was referred to for heat conservation for the HTF flowing in each pipe of the solar collector:

$$\frac{dT_f}{dt} = \left(\frac{2 \cdot \dot{m}_{p,f}}{\rho_f \cdot A_{p,i} \cdot L_p}\right) \cdot (T_{f,in} - T_f) + \left(\frac{1}{\rho_f \cdot c_f \cdot A_{p,i} \cdot R_{fp}}\right) \cdot (T_{p,i} - T_f) \tag{2}$$

where T_f is the average value of the HTF temperature in each pipe, $\dot{m}_{p,f}$ the mass flow rate of the fluid in each pipe, ρ_f the density of the fluid, $A_{p,i}$ the (internal) cross-sectional area of each tube, L_p the length of each pipe, $T_{f,in}$ the entering HTF temperature, c_f the specific heat of the HTF and R_{fp} the convective thermal resistance (per unit of length) between fluid and inner pipe wall. Due to the multi-physics approach of the finite element software, the above-mentioned ODE can be solved (in terms T_f as a function of time t) in parallel with the other PDEs (one for each layer of the road thermal collector). The two terms that allow the coupling between the solid domain of the pipe and the fluid domain contained therein are the (unknown) temperature value of the pipe internal wall $T_{p,i}$ and the heat flux (per unit of surface) $\dot{q}_{fp}$ imposed at the same boundary. The latter term (also an unknown) depends on both T_f and $T_{p,i}$ through the following relationship:

$$\dot{q}_{fp} = \frac{T_{p,i} - T_{f,a}}{\pi \cdot D_{p,i} \cdot R_{fp}} \tag{3}$$

where D_p is the internal diameter of the pipe. Therefore, to solve the problem, in addition to the geometrical characteristics of the solar collector (e.g. length L_p, layer thickness, pipe diameter D_p etc.) and the thermophysical properties of its materials, it is also necessary to define the thermophysical properties of the HTF (ρ_f and c_f) and the value of its flow rate $\dot{m}_{p,f}$ on which the R_{fp} term also depends (which can be calculated using empirical literature correlations for forced convection in circular tubes [33]).

Finally, referring to what is described in Fig. 2, the following surface energy balance was used as upper boundary condition (asphalt-atmosphere interface) of the FE model domine [7]:

$$\dot{q}_{sun} - \dot{q}_{rad} - \dot{q}_{conv} - \dot{q}_{cond} = 0 \tag{4}$$

where $\dot{q}_{sun}$ is the contribution related to the global solar irradiance incident on the asphalt surface, $\dot{q}_{rad}$ the heat losses from the long-wave radiative exchange, $\dot{q}_{conv}$ the convection heat losses and $\dot{q}_{cond}$ the heat transmitted by conduction from the surface into the asphalt-binder layer (assumed positive if entering). The relationships that were defined to estimate the different contributions that appear in Eq. (4) are described in detail below.

During daylight hours, the RTC upper surface is exposed to solar irradiance, which contributes to providing thermal gains that can be estimated using an expression of the following form:

$$\dot{q}_{sun} = G_h \cdot a_a \tag{5}$$

where G_h is the global horizontal solar irradiance and a_a the solar absorptance of the asphalt-binder layer. To quantify the net radiative heat power exchanged between the upper surface of the RTC and the environment, it is possible to use the Stefan-Boltzmann equation:

$$\dot{q}_{rad} = \sigma \cdot \varepsilon_a \cdot \left(T_a^4 - T_{sky}^4\right) \quad (6)$$

where σ is the Stefan–Boltzmann constant, ε_a the long-wave emissivity of the asphalt-binder surface, T_a the temperature of the asphalt-binder surface (in K) and T_{sky} the sky temperature (in K). The sky temperature T_{sky} (in K) can be related to the ambient temperature T_{air} (in K) through the following relationship [34,35]:

$$T_{sky} = \varepsilon_{sky}^{0.25} \cdot T_{air} \quad (7)$$

where ε_{sky} is the emissivity of the sky. In this study, the following expression elaborated by Ref. [36] through a reparameterization of the original model by Ref. [37] is adopted to model the sky emissivity:

$$\varepsilon_{sky} = [-0.4373 + 0.0037 \cdot (T_{air} + 273.15) + 0.0027 \cdot RH] \quad (8)$$

where RH is the relative humidity (in %). The convective heat losses of Equation (4) can be defined as a function of the temperature difference between the asphalt-binder layer and the air using the following relationship:

$$\dot{q}_{conv} = h_a \cdot (T_a - T_{air}) \quad (9)$$

where h_a is the convective heat transfer coefficient. In this study, this coefficient was related to wind speed v_{wi} through the following empirical correlation proposed by the Australian Standards [38]:

$$h_a = 3.1 + 4.1 \cdot v_{wi} \quad (10)$$

Wind speed values are normally measured by anemometers that are placed, in general, at different heights from those at which the wind speed values used for calibrating the empirical correlations were derived. For this reason, corrections must be made to the wind speed values measured by the climate stations (usually at an height of 10 m).

To account for the variations in wind speed at different heights above the ground, it is possible to use the following power law equation [39]:

$$v_{wi} = v_{wi,ref} \cdot \left(\frac{z}{z_{ref}}\right)^{\beta} \quad (11)$$

where $v_{wi,ref}$ is the wind velocity measured at a reference height z_{ref}, z [m] the height at which the speed must be evaluated and β the power-law exponent. This exponent is dependent on both the terrain roughness and the atmospheric stability conditions. In this model, it is assumed that β can be interpolated between the value associated with a smooth surface β_{ru} (rural areas) and the value associated with a rough surface β_{ur} (urban areas) using the following relationship:

$$\beta = \beta_{ru} + (\beta_{ur} - \beta_{ru}) \cdot ro \quad (12)$$

where ro is a parameter ranging from zero to one, representing the average surface roughness of the area ($ro = 0$ for smooth surfaces and $ro = 1$ for rough surfaces). The two values β_{ru} and β_{ur} can then be calculated from the identification of the atmospheric stability class using a recently proposed methodology [32]. It is noteworthy that the proposed approach for the determination of surface convective exchanges as a function of wind speed profile atmospheric stability conditions is proposed for the first time in a thermal model for RTC systems and, more generally, for road pavements. This approach, as already demonstrated in Ref. [32], emphasises the fact that local ventilation conditions, as opposed to those in which wind speeds are measured, can have a non-negligible effect on the extent of heat exchange.

Finally, the last term appearing in Eq. (4), representing heat flux that from transmitted, by conduction, to the asphalt-binder layer of the RTC, can be modelled through Fourier's law as:

$$\dot{q}_{cond} = \lambda_a \cdot \left.\frac{\partial T}{\partial z}\right|_{z=0} \quad (13)$$

where λ_a is the thermal conductivity of the asphalt-binder layer.

To summarize, the upper boundary condition of the FE domine is a complex function of the atmospheric variables G_h, T_{air}, RH and v_{wi}, which are either measured locally through a weather station or extracted from a TMY of the collector location.

2.2. Construction and material properties of the new road thermal collector

Fig. 3 shows the installation of the 16 pipes (19 m long) above the insulating layer of the new SMARTEP collector. These pipes (which have a diameter of 0.032 m and a thickness of 0.29 cm) are made of high-density cross-linked polyethylene (PEX-A) and are arranged horizontally, at a depth from the surface of 14.5 cm and with a distance of 25 cm between each other. Moreover, referring to Table 1, the collector stratigraphy from top to bottom is composed as follows.

- the asphalt-binder layer (11 cm), composed of bituminous mixture, aggregates, and additives. The volumetric fractions of the bituminous mixture are as follows: 12 % bitumen, 83.5 % aggregates, and the remaining 4.5 % void volume.
- the conductive concrete layer (7 cm), in which the pipes have been inserted. Its function, besides providing support, is to enhance conductive heat exchange.
- the insulating concrete layer (50 cm), designed to reduce conductive heat losses downward. The low thermal conductivity is achieved by incorporating EPS (Expanded Sintered Polystyrene) as an aggregate in the concrete (ISOCRETE® mix).

Through the numerical experimental analyses presented in a previous work [7], the thermophysical properties of each distinct solid layer composing the collector and its pipes were assessed (see Table 1).

Through the numerical experimental analyses presented in a previous work [7], the thermophysical properties of each distinct solid layer composing the RTC and its pipes were assessed (see Table 1). Given λ and α, after estimating the bulk density ρ values of the different materials, the specific heats of Table 1 were then calculated using the following relationship:

$$\dot{q}_{cond} = \lambda_a \cdot \left.\frac{\partial T}{\partial z}\right|_{z=0} \quad (14)$$

where it is emphasized that specific heat in the case of dry porous media always coincides with the specific heat of the solid phase c_s. In other words, this physical property is constant and does not change with porosity (or bulk density) of the material.

To accurately define the relation between the thermal conductivity

Fig. 3. Installation of the pipes of the SMARTEP RTC and connection with the manifolds.

Table 1
Geometrical and thermophysical properties of the RTC layers and HEPs.

material type	thermal conductivity	specific heat	density	thickness
	[W·m^{-1}•K^{-1})]	[kJ·kg^{-1}•K^{-1})]	[kg·m^{-3}]	[m]
Asphalt-binder	0.95	1314	1545	0.11
Conductive concrete	1.83	950	2250	0.07
Lightweight concrete	0.95	838	2055	0.5
Soil base	1.175	1302	1804	–
Pipes (PeX-A)	0.42	2300	932	0.003

of conductive and lightweight (insulating) concrete and their bulk density, two empirical correlations relating these quantities via a power function were identified in the literature [40]. Two of these correlations are depicted in Fig. 4 (blue and green lines) along with the experimental data (black circles in the figure) provided by the manufacturer of the insulating cement ISOCRETE® that was used in the studied RTC. Then, from this experimental data, the following new correlation was extrapolated (red line in Fig. 4):

$$\lambda_{ins} = 0.7337 \cdot e^{0.0012 \cdot \rho_{ins}} \quad (15)$$

Using this correlation, the bulk density value of road thermal collector insulation material (see Table 1) was assessed from its thermal conductivity value (point A in Fig. 4). This bulk density value was then entered into Eq. (14), together with both the diffusivity and thermal conductivity of this material, to calculate its specific heat. Eq. (15) was also used to estimate what the conductivity of the same material would have been if it had been prepared with a lower density (higher porosity).

Point B in Fig. 4 represents the lighter, less conductive material that was considered in the parametric analyses described below ($\rho_{ins} = 1400$ kg m^{-3} and $\lambda_{ins} = 0.42$ W m^{-1} K^{-1}). As mentioned above, for both materials (A and B in Fig. 4) the specific heat remains identical and equal to $c_{ins} = 850$ J kg^{-1} K^{-1} (see Table 1).

Finally, for simulations, the results of which are shown below, for the asphalt-binder surface layer a solar absorptance $a_a = 0.932$ and a long-wave emissivity of $\varepsilon_a = 0.88$ was assumed using results of experimental tests conducted on this material [7]. These values are congruent with the ranges of absorptivity and emissivity values of this material that other studies assume in the range from 0.85 [11] to 0.93 [16].

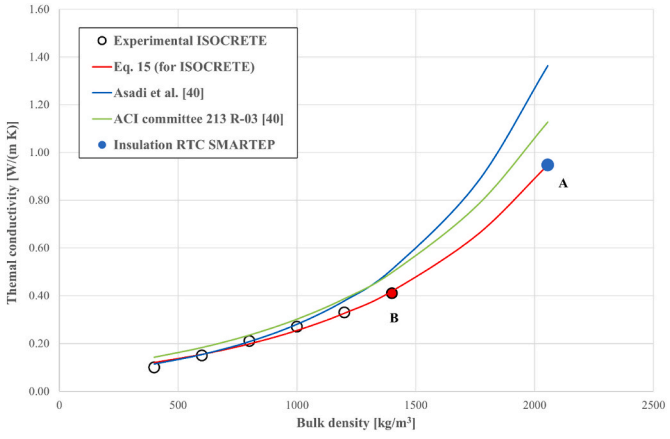

Fig. 4. Comparison of the new correlation between thermal conductivity and bulk density of ISOCRETE concrete with those estimated from the literature [40].

2.3. Thermal response tests on the road thermal collector and model validation

Fig. 5 depicts the facility test plant in Palermo (SMARTEP), illustrating the specific components of the installation. These include a BTES, the above-described solar collector, a dry-cooler, and the hydraulic loop connecting these elements. As shown in Fig. 5, the different components of the plant are instrumented with sensors, and a weather station has been also placed near the collector location.

Specifically, referring to Fig. 5, the following physical quantities can be monitored continuously.

- the air temperature T_{air}, the global irradiance on the horizontal surface G_h, the wind speed v_{wi} (measured at $z_{ref} = 4.30$ m above ground level), and the relative humidity RH (using the weather station located near the facility test site).
- The temperatures in the different layers of the RTC at different depths z along two vertical cross-sections (at the head and the tail of the collector). The mean values of the temperatures at the same depths in the two vertical sections are respectively indicated as T_A ($z = -0.02$ m), T_B ($z = -0.11$ m), T_C ($z = -0.145$ m), T_D ($z = -0.18$ m) and T_E ($z = -0.68$ m) in the following [7].
- The two temperatures T_1 and T_2 of the HTF at the dry-cooler inlet and outlet.

Between March 19, 2024 and March 25, 2024, an experimental campaign was carried out on this plant, the results of which were used to validate the FE model of the solar system presented above. At the end of this period, between March 23, 2024 and March 25, 2024, two TRTs were conducted on the road thermal collector in succession.

Each of these two tests was performed in two stages.

- **Phase 1**: during which the HTF recirculated continuously in the solar collector along the loop defined by a-b-c-d-e in Fig. 5 without any heat dissipation (dry-cooler off).
- **Phase 2**: during which the HTF circulated along the closed loop defined by a-b-c-d-e-f-g in Fig. 5 and the dry-cooler was turned on to allow the heat produced by the collector to be rejected into the environment.

The circulation pump that allowed the flow of heat transfer fluid was switched on between 9:45 a.m. on March 23, 2024 and 9:00 a.m. on March 25, 2024. The dry-cooler was switched on in two successive time intervals. The first interval was between 18:02 on March 23, 2024 and 7:18 on March 24, 2024 and the second between 21:33 on March 24, 2024 and 9:00 on March 25, 2024. A constant value of the circulating mass flow rate in the hydraulic circuit of 2973 kg/h was set during the two TRTs. During the entire period in which the experiment was conducted (from March 19, 2024 to March 25, 2024) All measured physical quantities were recorded.

After the experimental campaign, the FE model of the solar collector was employed to simulate the above-described experiment in terms of time changes in the temperatures of both the distinct RTC layers and the fluid circulating in the hydraulic circuit. For this aim, by analysing the recorded data, an empirical curve modelling the operation of the dry cooler was defined in which the difference between $T_1 - T_2$ was set as a function of $T_1 - T_{air}$. This relationship was then entered into the FE model to simulate the temperature reductions due to the heat sink.

For this purpose, the meteorological variables measured by the weather station during the experimental campaign were employed as input for the numerical model. Finally, the comparison between the experimental and numerical results permitted the model to be validated.

To assess the accuracy of the finite element simulation model, both MAE and MAPE were evaluated. MAE measures the absolute difference between the actual and predicted values and provides an average error

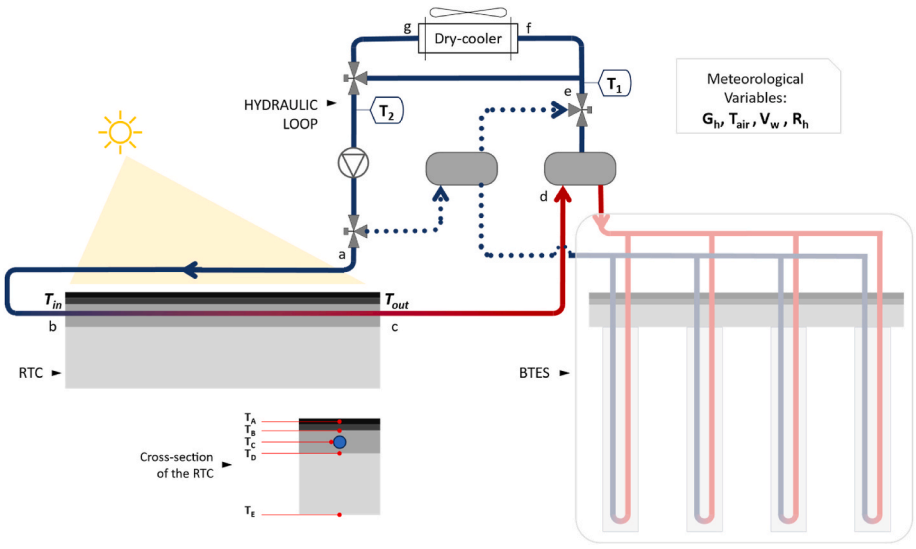

Fig. 5. Schematic layout of the facility test plant of Palermo (SMARTEP).

value and is defined as [41]:

$$MAE = \frac{1}{N}\sum_{j=0}^{N}\left|y_j - y\right| \tag{16}$$

where, N is the total number of samples in the dataset, and y_j and y are the actual value and predicted value of the target variable, respectively. MAPE, on the other hand, measures the percentage difference between the actual and predicted values and is defined as [42]:

$$MAPE = \frac{1}{N}\sum_{j=0}^{N}\left|\frac{y_j - y}{y_j}\right|\cdot 100 \tag{17}$$

2.4. Parametric numerical analysis to optimize road thermal collector configuration

After calibrating the FE model, a series of parametric numerical simulations were carried out by varying the thermophysical properties and thickness of the insulating concrete layer and the spacing between the exchanger pipes of the RTC. These analyses were aimed at identifying the collector configurations characterized by higher solar-to-thermal conversion efficiency to this end, it was assumed that all analyzed solar collector configurations have the same extent as the SMARTEP prototype with which they also share the thicknesses and physical characteristics of the two most superficial layers (asphalt-binder and conductive concrete).

Starting from these constraints, three possible inter-pipe distances were therefore considered: 0.20 m, 0.25 m and 0.33 m (which implies collectors with 20, 16, and 12 pipes respectively). Furthermore, for each of these three configurations, two possible thicknesses of the insulating material (located below the layer in which the pipes are embedded) were assumed to be 0.5 m and 0.25 m respectively. Moreover, for each of the above configurations, two possible bulk densities of the lightweight concrete (insulating material) were considered.

- Concrete A: $\rho_{ins} = 2055$ kg m^{-3}, $\lambda_{ins} = 0.95$ W m^{-1} K^{-1} and $c_{ins} = 850$ J kg^{-1} K^{-1} (identical to that of the RTC in Palermo).
- Concrete B: $\rho_{ins} = 1400$ kg m^{-3}, $\lambda_{ins} = 0.42$ W m^{-1} K^{-1} and $c_{ins} = 850$ J kg^{-1} K^{-1}.

In addition, for each of the three main groups of configurations (characterized by the same tube spacing), two more configurations (for a grand total of six) were added for comparison purposes: the first without an insulating layer the second with a perfectly adiabatic layer.

A total of 18 configurations of the road thermal collector were, therefore, studied as summarized in Table 2, where each of these is identified in terms of: pipe spacing, thickness and thermal conductivity of the insulating material, and number of pipes. In this table, for example, the configuration of the Palermo solar collector (SMARTEP) is identified as C1. For each of the 18 configurations, hourly dynamic simulations of the summer thermal energy production period (between April and October) were carried out using the FE model assuming a constant collector input temperature of 20 °C.

This temperature is approximately equal to the average annual air temperature value in Palermo). To perform these numerical analyses, the meteorological input variables were assessed an hourly basis using the TMY generated for Palermo using METEONORM [43].

Moreover, the mass flow rate of the heat transfer fluid of circulating in each pipe was set to $\dot{m}_f = 326$ kg h^{-1}. This value corresponds to a Reynolds number of about Re = 5000 (turbulent flux).

Finally, to simulate the daily turn-on and turn-off of the plant HTF circulation pump, a new control logic (which is currently being studied and tested in the Palermo collector) has been implemented in the numerical model. Specifically, it was assumed that the circulation pump is

Table 2
RTC configurations studied with the FE model.

name	pipes spacing [m]	insulation thickness [m]	thermal conductivity [W/(m K)]	pipe number
A1	0.20	0.50	0.95	20
A2	0.20	0.50	0.41	20
A3	0.20	0.00	–	20
A4	0.20	–	0.00	20
B1	0.20	0.25	0.95	20
B2	0.20	0.25	0.41	20
C1	0.25	0.50	0.95	16
C2	0.25	0.50	0.41	16
C3	0.25	0.00	–	16
C4	0.25	–	0.00	16
D1	0.25	0.25	0.95	16
D2	0.25	0.25	0.41	16
E1	0.33	0.50	0.95	12
E2	0.33	0.50	0.41	12
E3	0.33	0.00	–	12
E4	0.33	–	0.00	12
F1	0.33	0.25	0.95	12
F2	0.33	0.25	0.41	12

turned on only when the measured solar irradiance exceeds a minimum threshold (always set at $G_h = 50$ W m^{-2}).

On the other hand, the circulation pump turns off whenever the HTF temperature at the solar collector inlet is higher than the average temperature of the outer wall of the exchanger pipes embedded into the concrete layer (measured by the temperature sensor T_C in Fig. 5).

As described in detail below in this paper, the results of numerical simulations performed on the 18 RTC configurations (in terms of hot water produced temperatures, thermal power output, and energy harvested) were processed to assess.

- the parameters that most influence the solar-to-thermal conversion efficiency;
- the effectiveness in using a thermal insulation layer at the base of the RTC.

3. Results and discussion

This section presents the results of the TRTs carried out on the Palermo road thermal collector prototype, the validation of the two-dimensional FE model carried out using these data, and the results of the parametric analyses aimed at defining an optimized solar collector.

3.1. Results of the experimental campaign and comparison with numerical simulations

Fig. 6 presents a comparison of the entering and outlet HTF temperatures (T_2 and T_1, respectively) at the solar collector, along with the average pipe temperature (T_C) and air temperature (T_{air}) recorded during the experimental campaign. Based on the preliminary experimental results, the following observations can be made:

- on the four days before the execution of the TRTs (between March 19, 2024 and March 23, 2024) the water temperatures T_1 and T_2 were identical to each other and in equilibrium with the temperature of the air in the control room (where the thermal sensors, hydraulic connections, valves, and circulation pump are placed). These temperatures followed the variation of the external air temperature T_{air} with a delay of about 5 h (due to the inertia of the small building).
- Whenever the pump was turned on (Phase 1 of the TRTs) the two fluid temperatures T_1 and T_2 (still identical to each other) suddenly underwent an increase of about 8 °C and became close to T_C (the temperature of the outer wall of the pipes of the RTC).
- Finally, during the heat dissipation phase (Phase 2 of the TRTs), the differences between T_1 and T_2 (ranging from 0.2 °C to 1.2 °C) indicate that the dry-cooler was characterized by a cooling heat capacity of comprised between 0.69 kW and 4.16 kW.

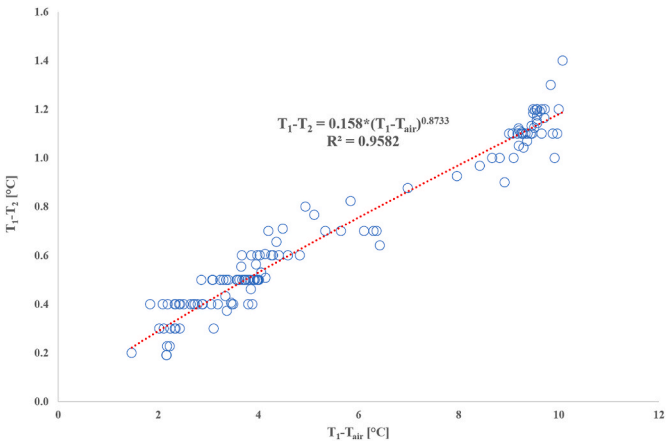

Fig. 7. Empirical characteristic curve of the dry cooler.

From the analysis of the temperatures T_1 and T_2 entering and leaving the dry cooler and considering the air temperature values, the following characteristic relationship of the dry cooler was defined:

$$T_1 - T_2 = 0.158 \cdot (T_1 - T_{air})^{0.8733} \quad (18)$$

This curve, which is only valid for the mass flow rate of water considered (2973 kg/h) was included in the COMSOL model, allowing the thermal jump imposed on the fluid in the solar collector model to be defined (see Fig. 7).

Fig. 8 depicts the temperature changes observed in the RTC layer at different depths over the same time period. These temperature curves illustrate the typical daily cyclic sinusoidal trend, with the progressive reduction in amplitude and phase shift of the temperature wave as depth increases.

Fig. 9 shows a comparison of the measured and simulated values (with the new FE model) of the temperature variations of sensor A

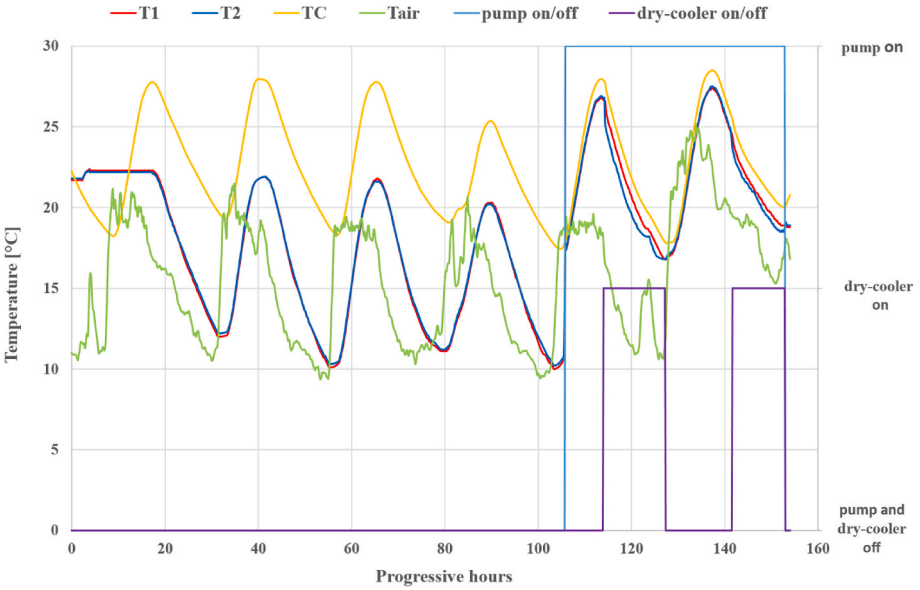

Fig. 6. Temperature variations of the HTF and the different layers of the RTC during the experimental campaign.

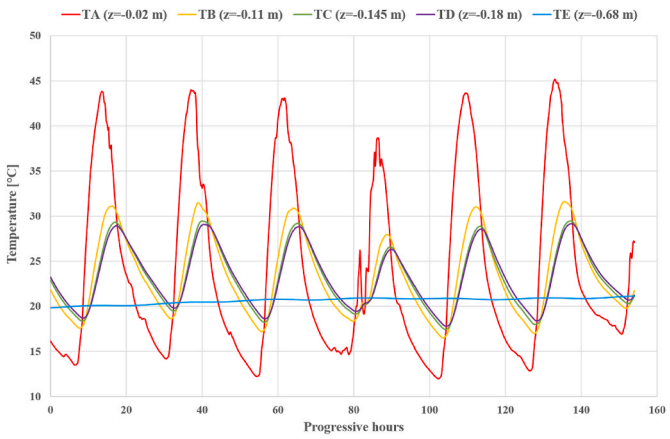

Fig. 8. Temperature variations in the RTC at different depths during the experimental campaign.

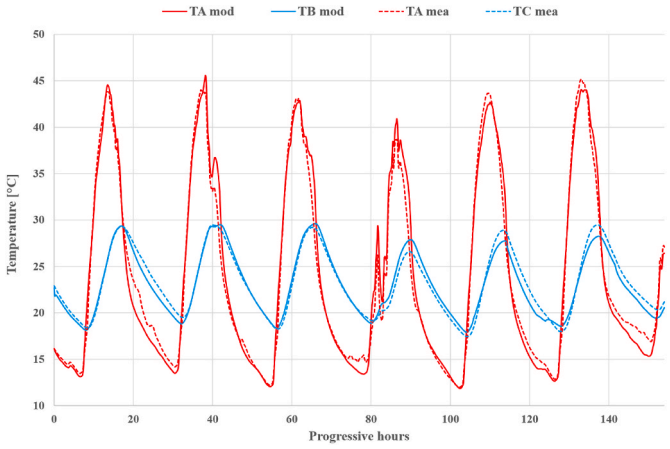

Fig. 9. Comparison of the measured and simulated values of the surface temperature T_A and the pipe temperature T_C during the experimental campaign.

(placed 2 cm below the pavement surface) and sensor B (which is deeper than the surface) during the entire experimental campaign. From this data, it is possible to estimate an $MAE = 1.10$ °C and a $MAPE = 4.76$ % for the whole period considered. On the other hand, for the deeper sensor B, a $MAE = 0.622$ °C and a $MAPE = 2.68$ % can be calculated. In general, these values indicate a good agreement between the simulated and modelled temperature data. However, the higher errors found in the estimation of the surface temperature could be due either to the lower accuracy of the measurements due to the interference of the sensor A with the atmosphere, or to the higher uncertainties of the calculated values of the surface energy balance equation (which is affected by the uncertainties of all the inputs measured by the weather station).

Shown in Fig. 10 is a comparison of the measured and simulated values of the water temperature variations at the inlet T_1 and outlet T_2 from the solar collector during the execution of the two TRTs. For comparison, the variation of the temperature measured at the outer wall of one of the pipes of the (T_C) is also plotted in the same figure. By comparing experimental and numerical data, it was possible to assess that the model can predict water temperature variations with a $MAE = 0.80$ °C and a $MAPE = 4$ %. However, from the same Fig. 10, comparing the measured variations in water temperature (T_1 and T_2) with those of the pipe (T_C) during Phase 1 of the TRT (recirculation only), it can be deduced that there are local thermal losses in the external pipes connecting the solar collector with the dry cooler. During Phase 1, in fact, the recirculating water should approximate that of the pipe in the RTC as no heat is extracted. Similar thermal losses will also occur in Phase 2 of

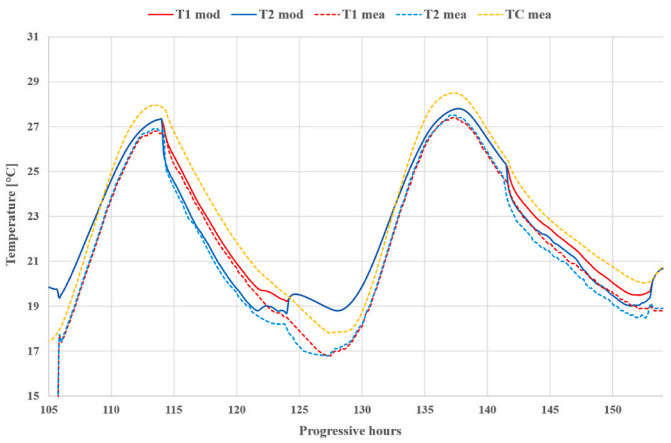

Fig. 10. Comparison of the measured and simulated values of the HTF temperatures during the execution of the TRTs.

the TRT during which the heat extracted from the solar collector is dissipated into the environment. In fact, as can be seen from Fig. 10 itself, the water temperatures simulated with the model during Phase 1 of both TRTs are always intermediate between those measured for the water and those measured in the pipe. In other words, it is plausible to argue that if the thermal losses that are concentrated in the hydraulic circuit connecting the RTC to the heat sink were also taken into account in the FE model, the accuracy of the model in predicting the operation of the solar collector would increase.

To summarize, considering the good agreement between the measured and modelled values of both the temperatures of the different layers in the RTC and the water circulating in the pipes throughout the experimental campaign, and also taking into account the uncertainties of the measurements made, it is possible to say that the FE model proposed with this study is sufficiently accurate to simulate the operation of this type of systems.

Furthermore, from this experimental campaign, it was also possible to assess that during the TRTs.

- the peak thermal output of the solar collector was about 2.254 kW (which, however, refers to a flow rate of 2973 kg h^{-1} lower than that which will be operational in the system, estimated to be 5500 kg h^{-1}).
- the total thermal energy produced by the collector amounts to 44 kWh in correspondence to a total solar energy input of about 710 kWh.

By rationing these last two quantities, it is possible to assess an average solar-to-thermal conversion efficiency of about 6 %. This last value of efficiency is compliant with what was expected for this collector both considering that the period of the year when these tests were carried out is characterized by relatively low solar insolation and taking into account that the fluid flow rate (and thus the convective exchange coefficient in the heat exchanger tubes) are lower than the expected operating values for the system.

3.2. Results of the parametric finite element simulations

The first unexpected outcome of the parametric simulations was that the thickness and the thermal conductivity values assumed for the insulation layer of the RTC in all the different studied configurations (see Table 2) had a minimal impact on both the seasonally simulated harvested energy and HTF thermal levels. For this reason, the results presented below are summarized by considering as representative only the three cases named B1, D1 and F1 in Table 2. These cases correspond, respectively, to configurations of the RTC characterized by pipe

distances of 0.20 m, 0.25 m and 0.33 m, respectively. Fig. 10 shows the monthly thermal energy production and solar-to-thermal conversion efficiencies of these three considered configurations. This data shows that the annual thermal productions per unit of surface of road solar collector increase from 267 kWh m^{-2} y^{-1} (for F1 case with tube distances of 0.33 m) to approximately 319 kWh m^{-2} y^{-1} (for B1 case with tube distances of 0.20 m) corresponding to seasonal solar-to-thermal efficiencies that pass from 21 % to 25 % respectively.

The monthly values of both thermal output and efficiency are higher in the central summer months, as shown in Fig. 11. More specifically, the efficiency in August rises from 26 % (case F1) to almost 31 % (case B1). However, it is worth noting that these values refer to the assumption of a constant inlet HTF temperature equal to 20 °C. This strongly idealized condition was assumed only to make a comparison between the different configurations studied.

If a higher inlet temperature had been chosen, these efficiency values would have been lower. Similar considerations can be made when observing the results of both peak and average monthly thermal powers for the same three configurations, which are depicted in Fig. 12. This data shows that in July, the most productive month of the season, the monthly average thermal power output increases from about 6.12 kW (F1 configuration) to 7.25 kW (B1 configuration) while the peak thermal powers, for the same configurations, passes from 12 kW to 17 kW respectively.

These numerical results confirm what is already known from the previous literature studies, namely, that reducing the distance between the exchanger tubes in RTC systems increases the solar-to-thermal conversion efficiency. However, this result does not answer why the effect of an insulation layer placed below the tube level did not substantially increase the yield of these collectors. To better understand this in Fig. 13, the thermal output powers on the three most productive days of the year (between July 21 and 23) for 8 RTC configurations studied were plotted. Specifically for the case of tubes spaced 0.20 m apart the configurations named A1, A2, A3 and A4 (see Table 2) and for those with tubes spaced 0.25 m apart the C1, C2, C3 and C4.

Among these, the configurations A3 and C3 correspond to the case where there is no insulating layer while A4 and C4 to the ideal case of a perfectly insulating medium. These latter results clearly show that the effect of the layer thermally insulating the exchanger tubes increases the peak heat output during daytime production hours. This increasing effect is more pronounced the closer the exchanger tubes are to each other. Conversely, during nighttime hours, the effect of the insulation layer reduces the thermal power that can be extracted from the collector. The overall result is that the net energy that can be daily extracted from the RTC in the two different configurations (insulated and not insulated) does not differ much. These results, however, could change by considering control logics of the road thermal collector different from that considered in this study (which involves, h24 circulation of HTF in the collector during the central months of the summer season) or by assuming higher collector inlet temperatures. For this reason, it is desirable to carry out further studies that can investigate this aspect.

As a practical recommendation for stakeholders, it is suggested that road solar collectors be constructed following the stratigraphy of conventional roads and car parks, with the pipes installed at a spacing of approximately 20 cm beneath the asphalt-binder surface layer. This configuration can provide efficient thermal performance while minimizing both construction and long-term maintenance costs. Furthermore, regulatory frameworks to support the adoption of this promising technology should be developed based on parametric numerical models, such as the one presented in this study, to account for the influence of varying climatic conditions on collector performance.

4. Conclusion

This paper presents a new two-dimensional numerical model developed using the finite element method and aimed at simulating the operation of road thermal collectors. The model was implemented with COMSOL Multiphysics® software and validated using an experimental campaign conducted on a new prototype of a road thermal collector developed within the project 'Sustainable Model and Renewable Thinking Energy Parking' (SMARTEP) in a car park on the campus of the University of Palermo (Italy). The SMARTEP solar collector, occupying approximately 80 m^2 of car park surface area, exhibits a distinctive design in comparison to other systems of the same type. The tubes comprising the heat exchangers are not directly embedded in the surface asphalt-binder layer but rather are situated at a depth of approximately 14.5 cm within an underlying layer of thermally conductive concrete. The purpose of this design choice was to make the stratigraphy of the collector very similar to that which is usually built in urban roads, limiting both construction costs and possible problems during maintenance. Furthermore, an additional 50-cm-thick layer of lightened concrete with reduced thermal conductivity was constructed in this prototype, serving as a thermally insulating layer and designed to enhance the efficiency of the collector. The FE model presented in this study considers the thermophysical properties of the various constituent materials. In addition, in this study a novel approach for determining surface convective heat exchanges in road thermal collector systems, based on wind speed profiles and atmospheric stability conditions is introduced.

The FE model was able to reproduce the results of two thermal response tests that were conducted on the prototype between 19 and March 25, 2024 with good accuracy. The results of the tests enabled the estimation of a peak thermal output of the solar collector of approximately 2.254 kW. However, this figure refers to a flow rate of 2973 kg h^{-1}, which is lower than that which will be operational in the system, estimated to be 5500 kg h^{-1}. Furthermore, a total of 44 kWh of thermal

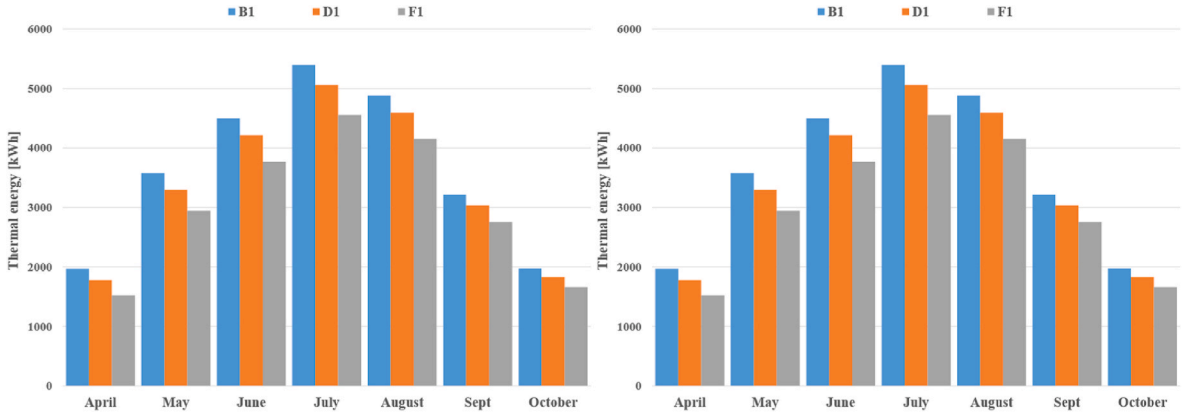

Fig. 11. Monthly values of thermal energy produced (left) and solar-to-thermal conversion efficiency (right) for RTC configurations named B1, D1 and F1.

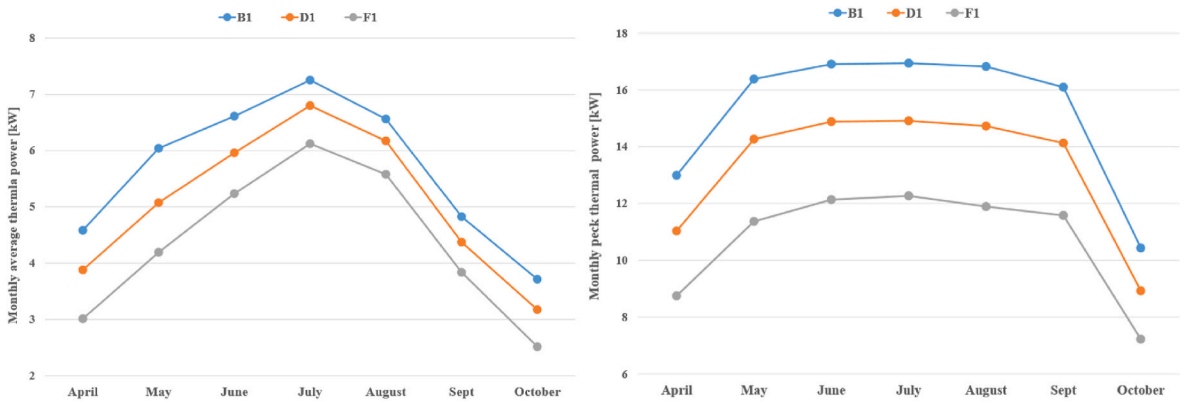

Fig. 12. Monthly values of the peck thermal power (left) and average thermal power for RTC configurations named B1, D1 and F1.

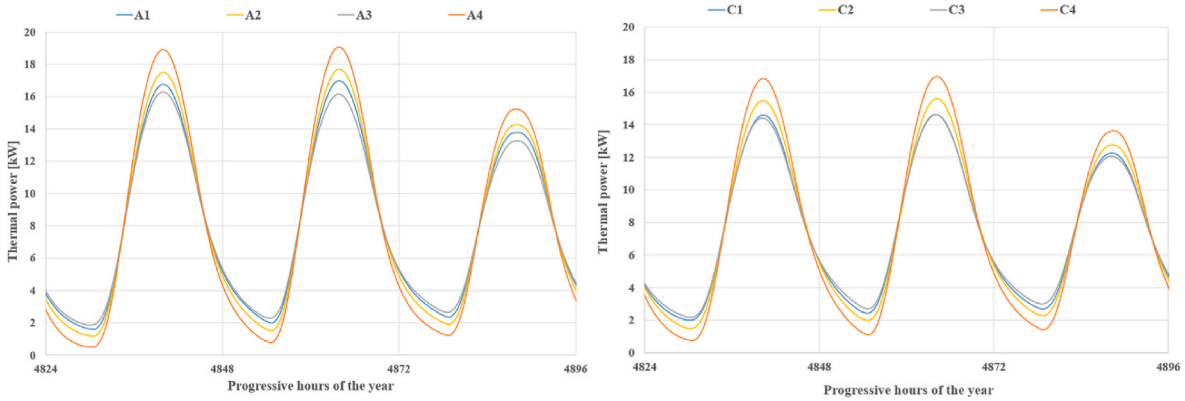

Fig. 13. Simulated thermal power variations for different RTC configurations (A1, A2, A3, A4, C1, C2, C3 and C4) on the days between 21 and 23 July.

energy was produced through the collector on the two testing days at a solar input of approximately 710 kWh. These values correspond to an average solar-to-thermal conversion efficiency of approximately 6 %. This percentage is consistent with the anticipated performance of this collector, given the relatively low solar insolation during the testing period and the reduced fluid flow rate (and thus convective exchange coefficient in the heat exchanger tubes) compared to the expected operating values for the system.

Following the validation of the FE model, a series of parametric simulations were conducted to assess the performance of 18 different collector configurations. These simulations were carried out assuming that these prototypes are located in Palermo, where the thermal energy production of each configuration was dynamically simulated. The configurations considered were defined considering all the possible combinations of three different distances between the exchanger tubes (33 cm, 25 cm and 20 cm, respectively), two thicknesses of insulating concrete (25 cm and 50 cm) and two thermal conductivities of the same concrete. The latter values were derived by defining a correlation to estimate the thermal conductivity of these materials as a function of their bulk density. The results of the aforementioned parametric analyses indicated that.

- the utilization of a layer of thermal insulation beneath that of the collector installation increases the peak heat output of these collectors during daytime hours of insolation, although this was accompanied by a reduction during the nighttime period (if the system was also operational after sunset). This tendency was found to be more pronounced the closer the heat exchanger tubes were to each other.
- Thus, on a seasonal basis, the net effect of using the insulating layer does not induce appreciable increases in collected thermal energy and thermal output levels.
- Conversely, the inter-tube spacing, as is already known from the literature, has an appreciable effect on the performance of this type of solar collector in that a relatively higher density per unit area of pipes increases both peak thermal output and harvested energy on a seasonal basis.

In conclusion, an enhanced configuration of the road thermal collector of Palermo could be achieved by arranging the tubes with closer spacing (approximately 20 cm) and eliminating the lightened thermal insulating concrete layer. For this enhanced collector, located in Palermo, a specific thermal production of approximately 320 kWh m^{-2} y^{-1} can be expected, corresponding to an average seasonal solar-to-thermal conversion efficiency of 25 %. These results were calculated considering an average inlet water temperature of 20 °C at the collector. In summary, adopting a conventional road stratigraphy with pipes placed about 20 cm below the asphalt-binder layer offers a cost-effective and efficient design for road solar collectors. Regulatory guidelines based on parametric modelling, as demonstrated in this study, are also recommended to support implementation under diverse climatic conditions. To this aim, further analysis should be conducted considering higher levels of heat transfer fluid temperature at the solar collector inlet.

CRediT authorship contribution statement

Alessandro Buscemi: Validation, Investigation, Writing – original draft, Conceptualization. **Stefania Guarino:** Data curation, Conceptualization, Formal analysis. **Alessandro Biondi:** Data curation, Formal analysis, Conceptualization. **Marco Beccali:** Data curation, Formal analysis, Conceptualization. **Valerio Lo Brano:** Data curation, Formal analysis, Conceptualization.

Declaration of competing interest

The authors declare that they have no known competing financial interests or personal relationships that could have appeared to influence the work reported in this paper.

Acknowledgment

This study was developed in the framework of the research activities carried out within the Project "Network 4 Energy Sustainable Transition — NEST", Spoke 8: Final use optimization, sustainability & resilience in energy supply chain, Project code PE0000021, Concession Decree No. 1561 of October 11, 2022 adopted by Ministero dell'Universita e della Ricerca (MUR), CUP UNIPA B73C22001280006. Project ' funded under the National Recovery and Resilience Plan (NRRP), Mission 4 Component 2 Investment 1.3 - Call for tender No. 341 of March 15, 2022 of Ministero dell'Universita e della Ricerca (MUR); funded by the European ' Union – NextGenerationEU.

Data availability

Data will be made available on request.

References

[1] Ritchie H. Sector by sector: where do global greenhouse gas emissions come from? Our World Data 2020. https://ourworldindata.org/ghg-emissions-by-sector.
[2] International Energy Agency. Tracking clean energy progress 2023 – analysis. IEA; 2023. https://www.iea.org/reports/tracking-clean-energy-progress-2023.
[3] International Renewable Energy Agency. World energy transitions outlook 2024: 1.5°C pathway. 2024.
[4] Zhang S, Ocłoń P, Klemeš JJ, Michorczyk P, Pielichowska K, Pielichowski K. Renewable energy systems for building heating, cooling and electricity production with thermal energy storage. Renew Sustain Energy Rev 2022;165. https://doi.org/10.1016/j.rser.2022.112560.
[5] Masrur H, Khaloie H, Al-Awami AT, Ferik S El, Senjyu T. Cost-aware modeling and operation of interconnected multi-energy microgrids considering environmental and resilience impact. Appl Energy 2024;356. https://doi.org/10.1016/j.apenergy.2023.122320.
[6] Mitali J, Dhinakaran S, Mohamad AA. Energy storage systems: a review. Energy Storage Sav 2022;1. https://doi.org/10.1016/j.enss.2022.07.002.
[7] Buscemi A, Beccali M, Guarino S, Lo Brano V. Coupling a road solar thermal collector and borehole thermal energy storage for building heating: first experimental and numerical results. Energy Convers Manag 2023;291. https://doi.org/10.1016/j.enconman.2023.117279.
[8] Bobes-Jesus V, Pascual-Muñoz P, Castro-Fresno D, Rodriguez-Hernandez J. Asphalt solar collectors: a literature review. Appl Energy 2013;102. https://doi.org/10.1016/j.apenergy.2012.08.050.
[9] Cui Y, Zhang F, Shao Y, Twaha S, Tong H. Techno-economic comprehensive review of state-of-the-art geothermal and solar roadway energy systems. Sustain Times 2022;14. https://doi.org/10.3390/su141710974.
[10] Ghalandari T, Hasheminejad N, Van den bergh W, Vuye C. A critical review on large-scale research prototypes and actual projects of hydronic asphalt pavement systems. Renew Energy 2021;177. https://doi.org/10.1016/j.renene.2021.06.010.
[11] Mirzanamadi R, Hagentoft CE, Johansson P. Numerical investigation of harvesting solar energy and anti-icing road surfaces using a hydronic heating pavement and borehole thermal energy storage. Energies 2018;11. https://doi.org/10.3390/en11123443.
[12] Nasir DSNM, Hughes BR, Calautit JK. A study of the impact of building geometry on the thermal performance of road pavement solar collectors. Energy 2015;93. https://doi.org/10.1016/j.energy.2015.09.128.
[13] Nasir DS, Pantua CAJ, Zhou B, Vital B, Calautit J, Hughes B. Numerical analysis of an urban road pavement solar collector (U-RPSC) for heat island mitigation: impact on the urban environment. Renew Energy 2021;164. https://doi.org/10.1016/j.renene.2020.07.107.
[14] Gu X, Makasis N, Motamedi Y, Narsilio GA, Arulrajah A, Horpibulsuk S. Geothermal pavements: field observations, numerical modelling and long-term performance. Geotechnique 2022;72:296. https://doi.org/10.1680/jgeot.20.
[15] Jaiswal P, Anupam BR, Chandrappa AK, Sahoo UC. Harvesting heat energy using geothermal and hydronic pavements for sustainable cities: a comprehensive review of an emerging idea. Sustain Cities Soc 2023;93. https://doi.org/10.1016/j.scs.2023.104539.
[16] Saleh NF, Zalghout AA, Sari Ad Din SA, Chehab GR, Saad GA. Design, construction, and evaluation of energy-harvesting asphalt pavement systems. Road Mater Pavement Des 2020;21:1647–74. https://doi.org/10.1080/14680629.2018.1564352.
[17] Van Bijsterveld WT, Houben LJM, Scarpas A, Molenaar AAA. Using pavement as solar collector: effect on pavement temperature and structural response. Transp Res Rec 2001. https://doi.org/10.3141/1778-17.
[18] Mallick RB, Chen BL, Bhowmick S. Harvesting energy from asphalt pavements and reducing the heat island effect. Int J Sustain Eng 2009;2:214–28. https://doi.org/10.1080/19397030903121950.
[19] Chiasson AD, Smith MD, Rees SJ. A model for simulating the performance of a pavement heating system as a supplemental heat rejecter with closed-loop ground-source heat pump systems. J Sol Energy Eng Trans ASME 2000;122. https://doi.org/10.1115/1.1330725.
[20] Xu H, Shi H, Tan Y, Ye Q, Liu X. Modeling and assessment of operation economic benefits for hydronic snow melting pavement system. Appl Energy 2022;326. https://doi.org/10.1016/j.apenergy.2022.119977.
[21] Johnsson J, Adl-Zarrabi B. A numerical and experimental study of a pavement solar collector for the northern hemisphere. Appl Energy 2020;260. https://doi.org/10.1016/j.apenergy.2019.114286.
[22] Songok J, Mäkiranta A, Rapantova N, Pospisil P, Martinkauppi B. Numerical simulation of heat recovery from asphalt pavement in Finnish climate conditions. Int J Therm Sci 2023;187. https://doi.org/10.1016/j.ijthermalsci.2023.108181.
[23] Motamedi Y, Makasis N, Gu X, Narsilio GA, Arulrajah A, Horpibulsuk S. Numerical investigation of geothermal pavements: design optimisation & boundary conditions. Transp Geotech 2022;37. https://doi.org/10.1016/j.trgeo.2022.100843.
[24] Carder DR, Barker KJ, Hewitt MG, Ritter D, Kiff A, others. Performance of an interseasonal heat transfer facility for collection, storage, and re-use of solar heat from the road surface, vol.302. Publ Proj Rep PPR; 2007.
[25] Ghalandari T, Ceulemans D, Hasheminejad N, Guldentops G, Van den bergh W, Verhaert I, et al. A simplified model to assess the thermal performance of pavement solar collectors. Appl Therm Eng 2021;197. https://doi.org/10.1016/j.applthermaleng.2021.117400.
[26] Ghalandari T, Baetens R, Verhaert I, Snm Nasir D, Van den bergh W, Vuye C. Thermal performance of a controllable pavement solar collector prototype with configuration flexibility. Appl Energy 2022;313. https://doi.org/10.1016/j.apenergy.2022.118908.
[27] Comsol, Multiphysics. Comsol - software for multiphysics simulation. COMSOL Multiphys/Heat Tranf Modul 2021:217–8. http://www.comsol.com.n.d.
[28] Morita K, Tago M. Operational characteristics of the GAIA snow-melting system in ninohe, Iwate, Japan. Geo Heat Cent Bull 2000;21:5–11.
[29] Farzan H, Zaim EH, Ameri M, Amiri T. Study on effects of wind velocity on thermal efficiency and heat dynamics of pavement solar collectors: an experimental and numerical study. Renew Energy 2021;163. https://doi.org/10.1016/j.renene.2020.10.087.
[30] Motamedi Y, Makasis N, Gu X, Narsilio GA, Arulrajah A, Horpibulsuk S. Investigating the thermal behaviour of geothermal pavements using thermal response test (TRT). Transp Geotech 2021;29. https://doi.org/10.1016/j.trgeo.2021.100576.
[31] Amico AD, Ciulla G, Buscemi A, Panno D, Zinzi M, Beccali M. Road thermal collector for building heating in south Europe. pdf; 2022. p. 1–24.
[32] Buscemi A, Biondi A, Catrini P, Guarino S, Lo Brano V. A novel model to assess the energy demand of outdoor swimming pools. Energy Convers Manag 2024;302. https://doi.org/10.1016/j.enconman.2024.118152.
[33] Gnielinski V. On heat transfer in tubes. Int J Heat Mass Tran 2013;63. https://doi.org/10.1016/j.ijheatmasstransfer.2013.04.015.
[34] Gliah O, Kruczek B, Etemad SG, Thibault J. The effective sky temperature: an enigmatic concept. Heat Mass Transf Und Stoffuebertragung 2011;47. https://doi.org/10.1007/s00231-011-0780-1.
[35] Evangelisti L, Guattari C, Asdrubali F. On the sky temperature models and their influence on buildings energy performance: a critical review. Energy Build 2019;183. https://doi.org/10.1016/j.enbuild.2018.11.037.
[36] Guo Y, Cheng J, Liang S. Comprehensive assessment of parameterization methods for estimating clear-sky surface downward longwave radiation. Theor Appl Climatol 2019;135. https://doi.org/10.1007/s00704-018-2423-7.
[37] Carmona F, Rivas R, Caselles V. Estimation of daytime downward longwave radiation under clear and cloudy skies conditions over a sub-humid region. Theor Appl Climatol 2014;115. https://doi.org/10.1007/s00704-013-0891-3.
[38] Australian Standards (3634 -1989). Solar heating systems for swimming pools. Sydney, Australia: North; 1989.
[39] Abubaker A, Kostić I, Kostić O. Numerical modelling of velocity profile parameters of the atmospheric boundary layer simulated in wind tunnels. IOP Conf Ser Mater Sci Eng 2018;393. https://doi.org/10.1088/1757-899X/393/1/012025.
[40] Asadi I, Shafigh P, Abu Hassan ZF Bin, Mahyuddin NB. Thermal conductivity of concrete – a review. J Build Eng 2018;20. https://doi.org/10.1016/j.jobe.2018.07.002.
[41] Willmott CJ, Matsuura K. Advantages of the mean absolute error (MAE) over the root mean square error (RMSE) in assessing average model performance. Clim Res 2005;30:79–82.
[42] Hyndman RJ, Koehler AB. Another look at measures of forecast accuracy. Int J Forecast 2006;22:679–88.
[43] Meteonorm. Meteonorm - global meteorological database. Meteotest; 2012.